An Enhanced Optical Coherence Microscope for the Study of Dynamic Processes in the Early Development of Plants and Animals

Project Description

1. Introduction

Optical coherence microscopy (OCM) is a non-invasive technique developed during the last decade to image biological tissue to depths of 1 to 2 mm. The strong light-scattering property of most tissue renders these depths inaccessible to other light-based methods, e.g., confocal or two-photon microscopy. Multiply-scattered light that would otherwise degrade images at these depths is rejected by the coherence gate of an OCM interferometer. With the help of previous NSF support (Sept 1996 through May 2000), we built an OCM instrument designed specifically to study critical events in the early development of plants and animals. The strength of our OCM lies in its ability to acquire 3-dimensional (3-D) images that can follow dynamic processes in the same developing organism.

We have used our OCM to study the formation of leaves in the model plant system *Arabidopsis thaliana* and to record the process of gastrulation in the widely-studied frog *Xenopus laevis*. These studies have independent scientific motivation, but also have provided critical feedback on the performance and design of our OCM. We describe our instrument and the studies of developing organisms in more detail in Section 2, "Results from Prior NSF Support."

Our current instrument, which uses a superluminescent diode (SLD) operating at 850 nm, has a depth resolution of 15 μm (in air) and a lateral resolution of 5 μm. Typically our images reach depths of 350 to 500 μm (5 to 7 attenuation lengths) in plants and animals, well beyond the reach of conventional, confocal, or multi-photon microscopy. While the images we have obtained with the current instrument are informative and encouraging, we need to improve our resolution by a factor of 2 or 3 and increase our depth penetration by 50% in order to make significant scientific contributions in developmental biology

In order to accomplish this, we propose to build a new version of our OCM instrument with a more powerful light source operating at a longer wavelength (1300 nm) for greater depth penetration. Our measurements in developing plants and animals suggest that the move from 850 nm to 1300 nm will increase the optical attenuation length by about 35%. We will collaborate with a commercial firm, Kapteyn-Murnane Laboratories, to design a kit for a chromium:forsterite (Cr^{4+}:Mg_2SiO_4) laser that operates at 1300 nm with an output power of at least 10 mW. The increased power over our current SLD source will result in a gain of two attenuation lengths in depth penetration. The combined effect is to increase the depth penetration by about 50%. The laser output will possess a spectral width of 150 nm yielding a depth resolution of 5 μm in air, a factor of 3 improvement over our current SLD. A Cr:forsterite laser meeting these specifications is not currently manufactured by a commercial vendor, but KM Labs will market our proposed laser so that it is available to other researchers.

In addition, we propose to add to the design of the new instrument two capabilities that promise to increase significantly the information content of the OCM images. First, we will incorporate a Doppler mode of operation which will enable the measurement of directed motion and/or diffusion of scatterers. In collaboration with Dr. Zhongping Chen at Beckman Laser Institute on the campus of UC Irvine, we acquired preliminary Doppler images of gastrulation in frog embryos that clearly show the Brownian motion of yolk platelets in the endodermal cells. The random motion of these roughly 1 μm diameter scatterers imparts remarkably improved contrast between the endodermal cells and the overlying ectoderm and mesoderm (see Section 3). The measured diffusive motion complements the traditional backscattered intensity and has given us much clearer time-lapse OCM movies of gastrulation.

As a second additional capability, we will implement rapid fine adjustment of the position of the focused beam waist in the sample, which will permit the measurement of refractive index variations in the sample. Previous researchers (Knuttel et al. 2000) have found that refractive index images add significant functional information to OCM images of skin. Similar increases in information and image quality should be obtained in developing organisms, especially in plants where large variations in refractive index occur. Both the refractive index and scatterer motion can serve as important intrinsic contrast agents in undifferentiated tissue whose cells are not readily distinguished by the amount of light they backscatter.

2. Results from Prior NSF Support

Our previous NSF grant (DBI 9612240), "Optical Coherence Microscopy in Developmental Biology," was awarded by the special Optical Science and Engineering Program and administered by the Instrument Development for Biological Research (IDBR) Program in the Division of Biological Infrastructure (DBI). Our primary goal was to construct an OCM to image critical events in the early development of plants and animals. Since spatial relationships between cells and groups of cells are important in the development of tissue, our OCM was designed specifically to produce 3-D images that can be rotated on a computer screen to achieve a 3-D perspective. The results of our work can be divided into two areas: (1) the design and performance of our OCM instrument, and (2) insights gained from our OCM images of developing frogs (*Xenopus laevis*) and plants (*Arabidopsis thaliana*).

Performance of Our OCM Instrument Our current OCM instrument provides the resolution and speed of image acquisition necessary to follow *in vivo* and in real time the development of an individual plant or frog. The design principles of our OCM (Fig. 1) and most of the instrumental details are described in two publications (Hoeling et al. 2000, Hoeling et al. 2001). We will summarize the most critical performance specifications.

The depth resolution of our OCM is 15 μm (full-width-at-half-maximum (FWHM)) in air, or 11 μm in tissue (with n = 1.4). The depth resolution is determined by the coherence length of the 850-nm SLD used as a light source. The lateral resolution of 5 μm (FWHM) corresponds to the waist diameter of the focused beam. A typical cell size in developing plants and animals is 5 to 10 μm, so individual cells can sometimes be resolved. A pair of galvoscanning mirrors moves the beam waist quickly over the x-y plane, then the focusing lens is stepped down along the z-axis (depth) and a slightly deeper x-y plane is scanned. At the same time the focusing lens is

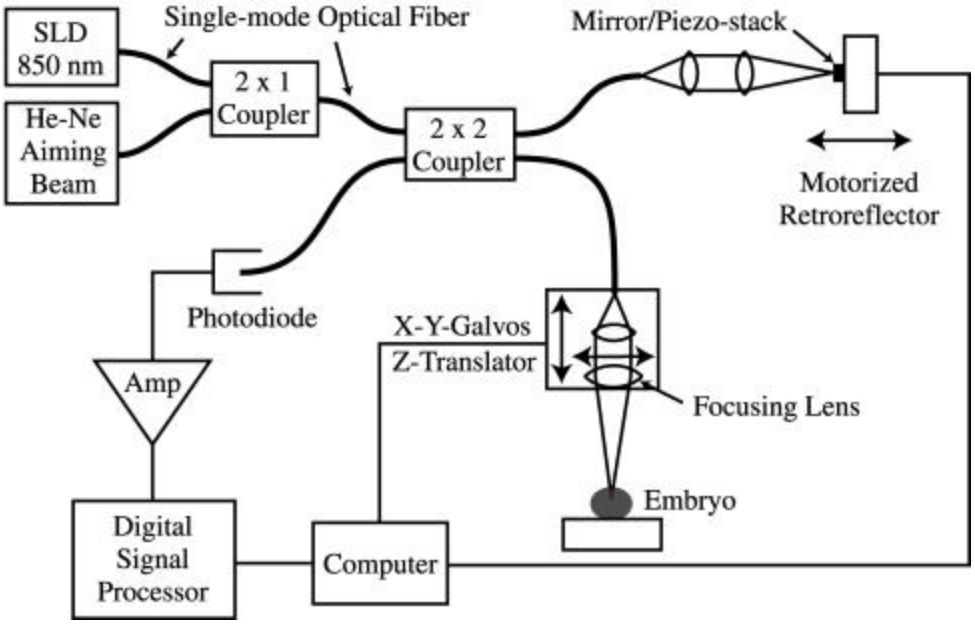

Fig. 1. Optical schematic of the current OCM instrument.

moved, the reference mirror is translated to keep the equal path length position of the OCM interferometer coincident with the focused beam waist. This latter procedure maintains the 5-μm lateral resolution throughout the depth of the sample.

Our OCM uses a novel, inexpensive, and robust method to produce rapidly oscillating fringes at the interferometer output. A tiny reference mirror (1.5 mm × 1.5mm × 0.1 mm) is glued to a small piezoelectric stack positioned at the rear of a cat's-eye retroreflector in the reference arm of the interferometer (Fig. 1). The reference beam is focused onto the mirror by the retroreflector lens, and the piezo stack is driven at its resonance frequency of 125 kHz to produce a phase modulation of roughly one fringe. (The small phase modulation is chosen to preserve the depth resolution.) The amplitude of the interference fringes at the output of the OCM is proportional to the square root of the power backscattered from the sample, and is ultimately the output signal of the OCM.

The performance of our OCM is limited by fundamental photon noise. We discovered that this noise is dominated by Bose-Einstein photon bunching, so we attenuated the reference beam by a factor of four to optimize the signal-to-noise ratio (Hoeling et al. 2000). Our use of a simple Michelson interferometer and a single photodetector was guided by convenience. Some researchers report an improvement with a Mach-Zehnder interferometer and a balanced receiver, albeit at the expense of instrument complexity (Rollins and Izatt 1999, Podoleanu 2000, Schmitt 1999). As we move to a more powerful light source, we will have to revise our interferometer configuration and use balanced heterodyne detection to circumvent photon bunching.

Finally, we recently replaced our analog signal processing electronics with a digital signal processing unit (DSP). The DSP provides flexibility in the trade-off between rapid image acquisition and image quality. We can now acquire a million-voxel image in roughly 1 minute, or we can scan more slowly and average out photon noise. Furthermore, the DSP samples the

entire fringe waveform and hence provides the phase of the fringes, thereby paving the way for the Doppler OCM mode of operation proposed in Section 3 (below).

The entire process of image acquisition is directed by computer programs written in the software environment of LabVIEW (National Instruments, Austin, TX). This graphical programming language runs on a Pentium III computer with a Windows NT 4.0 operating system. This is the same hardware/software platform used by our visualization software, making it possible in the future to acquire and visualize an OCM image on a single, relatively inexpensive computer.

We have written programs in the software environment of Visualization Express 5.0 (Advanced Visualization Systems, Waltham, MA) that allow us to "volume-render" our 3-D data sets onto a 2-D viewing screen (computer monitor). In this process, the contents of volume elements (voxels) are "blended" with the contents of voxels directly behind them to yield the final value assigned to a pixel on the viewing screen. An "opacity" parameter in this blending algorithm may be reduced to achieve a translucent appearance in which structures deep within the sample can be seen, or it can be increased to yield a superficial rendering of the sample. We find that rotating a translucent, volume-rendered 3-D data set is remarkably effective in producing a 3-D perspective. We can also rotate, slice, or crop the 3-D data set, yielding 2-D images that can be analyzed using standard methods. Often a 3-D perspective is used to determine the optimal 2-D slice to use in quantitative analyses. Hoeling et al. (2000) describes in more detail the operation of our visualization programs.

Frog Developmental Biology Our early OCM studies of frog development were performed on stage 41 frogs (approximately 3-day-old tadpoles) that had been lightly fixed (2% paraformaldehyde overnight at 4º C). Using one 3-D image collected from these fixed frogs we created a QuickTime movie that is included in Hoeling et al. (2000) and is also available on our website http://www.physics.hmc.edu/research/ocm.html. The movie illustrates the structure that

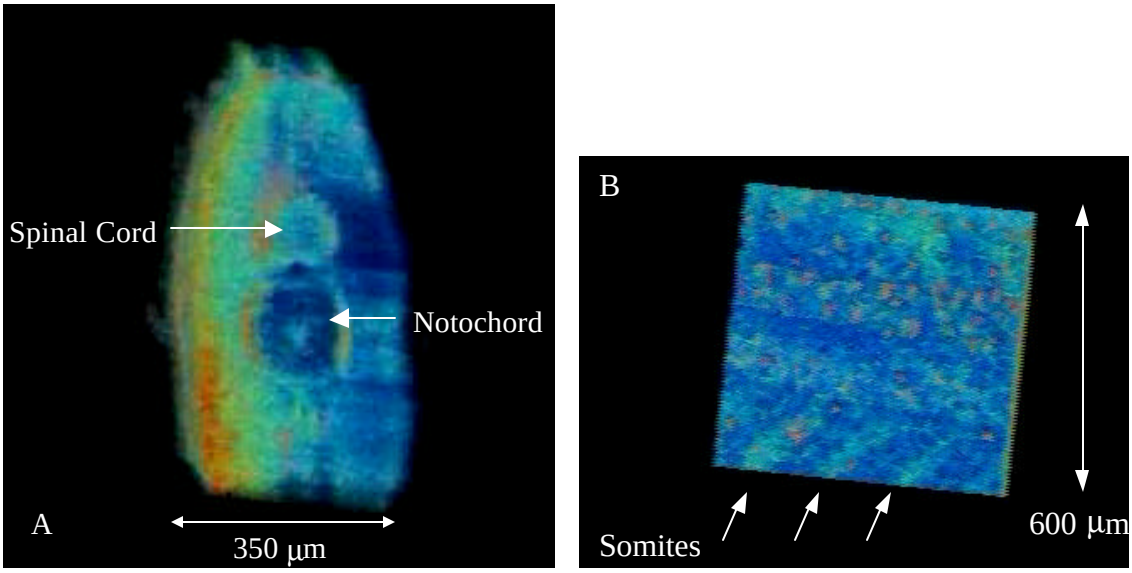

Fig. 2. OCM images of a frog embryo: (A) View along the spinal cord, (B) Side view obtained by rotating (A) by 90° about a vertical axis (Hoeling et al. 2000).

is evident and the 3-D perspective that can be achieved by rotating a volume-rendered image. The highly scattering spinal cord is clearly visible, and the degenerating notochord appears as a low-scattering cylinder. In a small range of viewing angles one can see directly down the notochord axis (Fig. 2A). Developing somites form diagonal stripes in a side-on view (Fig. 2B). The movie also illustrates the effect of altering the opacity value from a low, translucent setting to a high, superficial-view value. In these stage 41 frogs we measured an average attenuation coefficient at 850 nm of roughly 10/mm, yielding an attenuation length of 100 µm. We often imaged 400-µm deep into the frog tissue.

Our OCM studies during 1999 through 2001 focused on the development of live frogs during gastrulation (stages 10 to 13, 10 to 15 hours post fertilization). Attenuation at 850 nm is very high in these early stages of development, roughly 20/mm. Nevertheless, we are able to produce time-lapse movies from individual frog embryos of the involuting mesendodermal cells as they move below and across the ectodermal layer during gastrulation. These are the first movies to follow gastrulation in an individual embryo at this resolution and time scale. Fig. 3 contains two views near the end of gastrulation obtained from a single 3-D image. These views appear as corresponding frames in two time-lapse movies of gastrulation that are available on our website. The view in Fig. 3A is a vertical cross-section showing the mesendoderm moving from the periphery of the view toward a convergence spot near the top (animal pole) of the embryo. Fig. 3B is a top view looking down on the embryo. The top of the data set has been cropped off revealing the dark (low scattering) blastocoel fluid. Also visible at the periphery of the blastocoel fluid is a portion of the mesendoderm converging on a spot slightly to the lower right of the top (the animal pole) of the embryo. The sense of motion provided by the time-lapse movie is essential for a full appreciation of these 3-D images.

One goal of these studies is to test a model of gastrulation suggested recently (Winklbauer and Schurfeld 1999). The “vegetal rotation” described by these authors was seen in explanted slices of embryos; observing this vegetal rotation in intact embryos with our OCM would provide strong confirmation of this model. While our time-lapse movies are very encouraging, we will

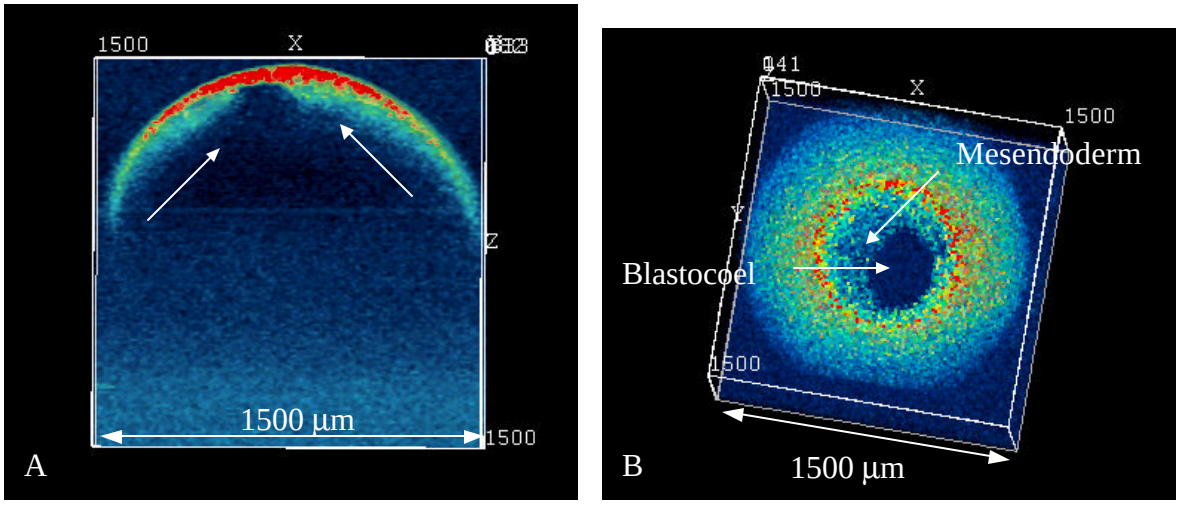

Fig. 3. Side-view (A) and top-view (B) near the end of gastrulation in a frog. Arrows in (A) indicate the direction of motion of the mesendoderm.

need about 50% more depth penetration to unambiguously test the suggestion of Winklbauer and Schurfeld. (See also Sections 3 and 4 below.)

Plant Developmental Biology Using our OCM, we have successfully followed the development of individual plants of *Arabidopsis thaliana* (Hettinger et al. 2000). This is the first study of plant development using OCM. We have focused on the shoot apex of the plant where a series of leaves are formed in a characteristic spiral pattern. Considerable effort in the plant biology community is being devoted to the study of the formation of this leaf pattern (phyllotaxy). Of particular interest is the relation between gene expression and the series of morphological changes in which leaf primordia emerge from the shoot apical meristem, a group of undifferentiated cells lying below the early leaves and embryonic cotyledons. In an intact plant the meristem and leaf primordia are shielded from the view of conventional light microscopes, so we used the OCM to monitor the appearance and growth of successive leaves during the development of an individual plant. The *Arabidopsis* plants, which were growing in soil throughout the experiment, showed no indication of damage or abnormal development despite many days of OCM imaging.

We found that *Arabidopsis* tissue is highly scattering; we measured an attenuation coefficient at 850 nm of roughly 15/mm corresponding to an attenuation length of 70 μm. We imaged typically 300 to 400-μm deep into tissue. For comparison, confocal fluorescence microscopy is limited to depths less than 100 μm. Our early imaging attempts were frustrated by the strong light-scattering of trichomes, hairlike structures on leaf surfaces. This problem was circumvented by using the glabrous1 (*gl-1*) mutant, which lacks trichomes. As a result, the OCM was able to follow readily the appearance and growth of successive leaves in the characteristic spiral pattern during development of a single plant. This is the first time that such a dynamic process has been followed at this depth in plant tissue. Images taken 10 minutes apart were virtually identical, but images taken an hour or two apart showed definite signs of growth. We noticed immediately that regions of high cellular activity are regions of high light scattering. Fig. 4 illustrates this finding. The meristem and the distal portion of the leaf primordium are highly active and highly scattering (red), though clearly there is surrounding and bridging tissue that scatters light less strongly (green or blue). This seems to be a very fortuitous result, imparting the role of optical probe to high cellular activity in developing organisms.

As we followed the appearance of successive leaf primordia in a particular plant, we noticed that the meristem seems to exhibit cycles of high and low light scattering, apparently phased with the production of primordia. This is a tentative finding. Our current spatial resolution is just shy of providing unambiguous discrimination between the meristem, leaf primordia, and associated stipules. We think that an improvement in resolution of a factor of 2 and slightly better depth penetration will allow us to record reliably the formation and separation of a leaf primordium from a meristem, and to resolve the question of dynamic cycling in the meristem.

Comparison of OCM images with scanning electron micrographs or histological sections of the same plant shows that OCM images are reliable, though they typically have poorer resolution than the electron micrographs and histological sections (Hettinger et al. 2000). On the other hand, producing the micrographs and sections destroyed the plant, preventing observation of subsequent development. We also used *Arabidopsis* mutants to test our OCM instrument.

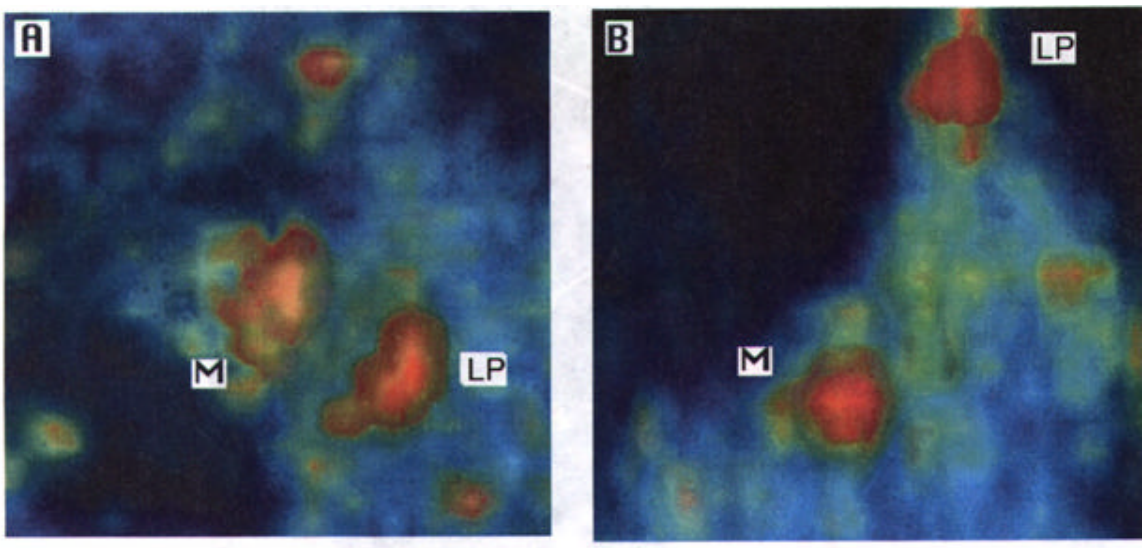

Fig. 4. (A) Top view (90 μm × 90 μm) and (B) side view (60 μm × 60 μm) of the shoot apex of a 9-day-old *Arabidopsis* plant. The OCM data set has been cropped to reveal the meristem (M) and a leaf primordium (LP).

Using the *shoot-meristemless* mutant, both OCM images and electron micrographs of the same plant show a void where the meristem should be.

3. The Improved and Enhanced OCM

We propose to build a new OCM instrument operating at 1300 nm with improved resolution and better depth penetration. The new instrument will also be able to detect the motion of scatterers and measure variations in the refractive index of the sample. Our current 850 nm OCM will receive modest upgrades and will be used to continue our studies of developing organisms while the new OCM is under construction.

Improved Light Source The choice of light source for the new OCM is a critical one - it determines the depth resolution and penetration of the instrument. We would like a source operating at roughly 1300 nm with an output power through a single mode fiber of at least 10 mW, and with a spectral width of approximately 150 nm (FWHM). Assuming a Gaussian spectrum, this corresponds to a depth resolution of 5 μm (FWHM) in air, a factor of 3 improvement over our current instrument. An output power of 10 mW through a single mode fiber will provide a factor of 10 increase over our current 850 nm SLD source. Though this higher power exceeds the safety level for scanning the human retina, it should have no harmful effects on typical tissue in developing plants and animals. The factor of 10 increase in power will provide more than two additional attenuation lengths of depth penetration. In addition the shift from 850 nm to 1300 nm will reduce the attenuation coefficient in frog embryos from 20/mm to 14/mm. The combined effects of longer wavelength and higher power will yield a 50% increase in depth penetration.

Until recently some groups of OCM researchers (Saxer et al. 2000, Rollins et al. 1998) employed an amplified SLD marketed by AFC Technologies (Hull, Quebec, Canada). This source operates

near 1300 nm with an output power of ~10 mW and with a spectral width of about 80 nm. Unfortunately the company was purchased by JDS Uniphase and the product has been discontinued. Other researchers have synthesized sources by combining two or more SLDs with different center wavelengths (Schmitt et al. 1997, Baumgartner et al. 1998, Zhang et al 2001). However, with commercially available 1300 nm SLDs or LEDs, it is impossible to meet our goals of 5 μm depth resolution and 10 mW output power.

Several research groups (Hartl et al. 2001, Chudoba et al. 2001, Zhang et al. 1998, Bouma et al. 1996) have developed Cr:forsterite lasers whose output characteristics are ideal for OCM. A broad spectrum is achieved by mode-locking the laser to produce short pulses. For example, a Gaussian pulse width of 17 fs (FWHM) ensures a spectral width of at least 146 nm (transform-limited pulse). If the laser output is coupled into a single-mode fiber, the fiber dispersion will broaden the pulse width, but the spectrum of the output will not narrow. Since the OCM depth resolution is a function of the spectral width, the preservation of short pulses is not essential for OCM. It is worth noting, however, that if the 17 fs pulse width is maintained, the short pulse duration results in a depth resolution of $(17 \text{ fs}) \times c / 2 = 2.5$ μm. We shall take a conservative approach and quote a depth resolution of 5 μm due to the 146 nm spectral width, and we will not assume that the pulse widths at the output of a laser will propagate intact.

Yanovsky et al. (1993) generated 25 fs pulses from a Cr:forsterite laser using a pair of SF6 prisms to minimize intracavity dispersion. The spectral width of the pulses was roughly 90 nm (FWHM) which would yield an OCM depth resolution of 8 μm. Again using a pair of SF6 prisms, Bouma et al. (1996) focused 100 mW of mode-locked output power from their Cr:forsterite laser into a dispersion-shifted single-mode fiber, broadening the output spectrum by nonlinear self-phase modulation. They measured a depth resolution of 6 μm (FWHM). By using SFS01 instead of SF6 prisms, Zhang et al. (1997) achieved 20 fs pulses. Later, Zhang et al. (1998) employed semiconductor saturable-absorber mirrors (SESAMs) to self-start the mode-locking of their Cr:forsterite laser, again producing 20 fs pulses. Recently Chudoba et al. (2001) used a pair of high-dispersion PBH71 prisms and double-chirped mirrors to produce 14 fs pulses at the output of their Cr:forsterite laser. The spectrum of the pulses contained a dip near the center wavelength (1400 nm), but the spectral width was roughly 200 nm (FWHM). The resulting depth resolution should be approximately 4 μm. Finally, Hartl et al. (2001) focused light from a mode-locked Ti:sapphire laser into an air-silica microstructure fiber and ultimately produced an output spectrum centered at roughly 1280 nm with a width of 370 nm (FWHM). The spectrum was nearly Gaussian and a depth resolution of 2.5 μm was demonstrated. Although none of these light sources is available commercially, it certainly appears to be technically feasible to achieve our goal of 5 μm depth resolution.

To our knowledge, there is only one commercial source of Cr:forsterite lasers. Avesta Project Ltd. (Moscow, Russia) markets a Cr:forsterite laser kit that is capable of 65 fs pulses. For a transform-limited Gaussian pulse, this corresponds to a 38 nm spectral width and a 20-μm depth resolution, four times worse than our goal of 5 μm. We propose to collaborate with a commercial firm, Kapteyn-Murnane Laboratories (KM Labs, Boulder, Colorado), to develop a stable, easy-to-assemble and easy-to-operate Cr:forsterite laser kit that will meet our OCM requirements. Drs. Henry Kapteyn and Margaret Murnane are recognized authorities in the field of ultrafast lasers, and they have expressed interest in designing a Cr:forsterite kit for use in

biological imaging. They currently market a very successful kit for titanium:sapphire lasers. Our plans are to keep the design simple and the instrument robust for easy commercialization, and to keep the price below $50k (including the pump laser).

Our development of a Cr:forsterite laser is also motivated by our desire to construct a hybrid 2-photon/OCM microscope for imaging in developmental biology. This is a separate collaborative project with Dr. Scott Fraser at Caltech. A single Cr:forsterite laser can supply the short pulses essential for 2-photon operation of the hybrid microscope, and the 1300 nm wavelength and substantial output power of the laser service both modes of operation. Two-photon microscopy can provide high resolution images at limited depths, and OCM can image more deeply though with lower resolution. Separate funding is being sought for the hybrid microscope, but clearly the results of our present development efforts will be directly applicable to that project.

OCM Interferometer Our current OCM (Fig. 1) directs only 25% of the SLD light to the sample. In order to maximize the signal-to-noise ratio, the final (reference) power incident upon the photodetector is reduced to just 3 μW out of an initial 1 mW of SLD source power (Hoeling et al. 2000). This seems wasteful of source power, and we must be certain to take full advantage of the higher power available from the proposed Cr:forsterite laser. Several researchers (Rollins and Izatt 1999, Podoleanu 2000, Schmitt 1999) have searched for the optimal OCM interferometer and photodetection scheme.

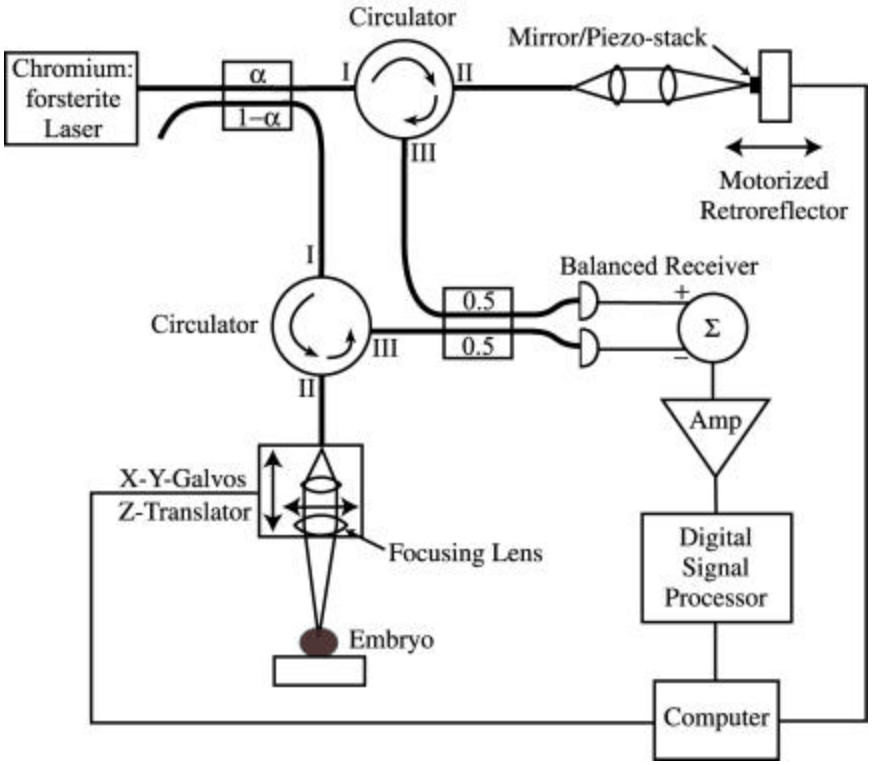

Fig. 5. Optical schematic of the proposed OCM instrument. A Mach-Zehnder interferometer is constructed with 3-port circulators, and balanced detectors are employed to reduce photon bunching.

We will follow the recommendation of Rollins and Izatt (1999) in constructing the new OCM—see Fig. 5. The configuration is basically a Mach-Zehnder interferometer with balanced detectors. The initial fiber coupler sends roughly 90% of the laser light ($1-\alpha \sim 0.9$) to the sample arm where it encounters a 3-port circulator. The circulator directs the light to the sample (port I to port II), and sends the light backscattered from the sample to the detectors (port II to port III). There is negligible cross-talk between ports of the circulator. Roughly 10% of the laser light ($\alpha \sim 0.1$) is directed to the 3-port circulator in the reference arm where it is sent to the retroreflector (port I to port II), and the reflected light is redirected to the detectors (port II to port III). The splitting ratio α of the initial fiber coupler will be chosen to maximize the signal-to-noise ratio for the specific components of the interferometer that we ultimately select and for the output characteristics achieved for the Cr:forsterite laser.

Light returning from the sample and reference arms is mixed and split equally between two detectors whose outputs are subtracted by a summing amplifier. This "balanced heterodyne detection" (Abbas et al. 1983) reduces the Bose-Einstein photon bunching that dominates the photon noise of both the SLD currently in use and the proposed Cr:forsterite laser. The term "relative intensity noise" is also used to describe Bose-Einstein photon bunching. This combination of balanced detectors and the unbalanced Mach-Zehnder interferometer will comprise a near-optimal use of photons generated by the Cr:forsterite laser.

Doppler OCM In collaboration with Drs. Zhongping Chen and Hongwu Ren at the Beckman Laser Institute (BLI), we used the BLI OCT to acquire images of developing frog embryos (see Fig. 6). Fig. 6A is a standard OCT image displaying the backscattered intensity from the tissue. Fig. 6B is constructed from the same fringe data as in Fig. 6A, but displays the standard deviations in the depth positions of scatterers during rapid successive line scans—red indicates scatterers whose positions varied greatly, and blue indicates scatterers that were relatively stationary. The BLI instrument records the OCT interferometer fringes and can extract the velocity of scatterers (along the beam) (Zhao et al. 2000). It can also identify those scatterers that possess zero mean velocity but execute Brownian motion and hence exhibit random fluctuations in velocity and position.

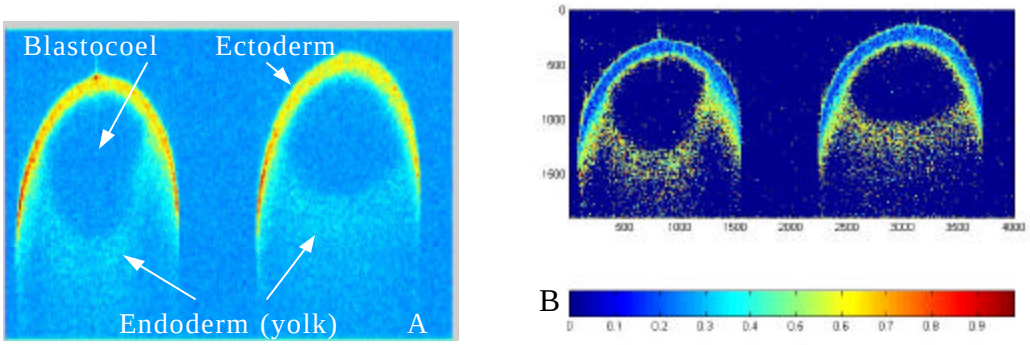

Fig. 6. Two-dimensional OCT images of two side-by-side developing frog embryos. Panel A is a standard intensity image, and B is a velocity variance image. The embryos are 1.2 mm in diameter. The BLI instrument operates at 1310 nm and uses the SLD from AFC Technologies mentioned in Section 2.

The yolk cells (endodermal cells) in Fig. 6B appear green, yellow, and sometimes red, indicating substantial random motion. The conventional velocity image (not shown) appears uniformly blue, indicating no directed motion in the embryos. We suspect that the yolk platelets, about 1 μm in diameter, are exhibiting Brownian motion within the yolk cells. Calculations of expected speeds and trajectories agree with the measured displacements. The result is a remarkable increase in contrast between the yolk cells and the ectoderm (cells forming the outer layer of the embryo). The improvement in image quality is even more striking in the time-lapse movies made of gastrulation (available on our website) in which the motion of the yolk cells can be seen to play an important role in the initiation of the sequence of events.

We propose to include a Doppler capability in the proposed new OCM. In the meantime we are modifying our existing 850 nm OCM to provide information on scatterer motion. We have the necessary equipment, but we will need to reprogram the DSP unit and calibrate the system with latex spheres executing Brownian motion in water. Extensive examination of tissue and cell cultures with the Doppler OCM will then be performed to be sure that we are indeed seeing diffusion of scatterers.

Most Doppler OCT researchers generate fringes by translating (at least effectively) the reference mirror (Yazdanfar et al. 1997, Chen et al. 1997, and see the review Chen et al. 1999). However, we generate fringes in our existing OCM (and will generate fringes in our proposed new instrument) by oscillating the reference mirror during an *en face* scan of the x-y (horizontal) plane. It must be emphasized that our *en face* method of scanning does not preclude us from performing Doppler measurements. The interference term (the fringe signal) of the output of our OCM is given by:

$$V(t) \propto 2\sqrt{P_{ref} P_{samp}} \cos\left[\frac{2p}{l}[2d_{mirror}(t) + 2z_{scatterer}(t)] + f(t)\right] \qquad (1)$$

where $d_{mirror}(t)$ is the position of the oscillating reference mirror, $z_{scatterer}(t)$ is the depth position (along the beam) of a scatterer, and $f(t)$ is a slow phase wander of the interferometer with a time scale of seconds or minutes. We drive a piezoelectric stack so that the position of the mirror obeys $d_{mirror}(t) = d_o \sin(w_{mod} t)$ where the modulation frequency is roughly 125 kHz. The phase changes in Eqn. (1) due to scatterer motion are usually slow compared to the piezo-driven phase modulation, and fast compared to the slow phase drift of the interferometer.

The factor P_{samp}, the power backscattered from the sample, varies for two reasons as the beam scans across the x-y plane. First, the tissue illuminated has a varying cross-section for backscattering. Second, the power incident upon a particular scatterer varies as the beam sweeps across it. This variation in the incident power may modulate the amplitude of the fringes from a particular scatterer, but the phase of the fringe signal depends only on the z-position of the scatterer, not on the x-position of the beam—see the phase of the cosine in Eqn. (1).

As a rapid x-scan is performed (typically a few milliseconds), the DSP unit digitizes the fringe signal and stores it in memory. As successive rapid x-scans are performed, it will be possible to calculate the change in phase of that portion of the fringe signal produced by a particular scatterer. The correlation function of successive fringe signals is often used to determine the

phase change (Yazdanfar et al. 2001). If the scatterer position is given by $z_{scatterer}(t) = v_z t$, then the phase of the fringe signal will increase linearly with time, and the velocity can be calculated by dividing the change in phase of the fringe signal by the time between x-scans. If, on the other hand, $z_{scatterer}(t)$ is a random function of time, then the phase of the fringe signal will change randomly between x-scans, yielding a mean of zero. However, the standard deviation of the phase changes over several successive x-scans will serve to characterize the diffusion or Brownian motion that is occurring. We think the measurement of scatterer motion will add significantly to the quality of our OCM images.

4. Studies of Gastrulation in the Frog (*Xenopus laevis*) and Phyllotaxy in Plants (*Arabidopsis thaliana*)

Section 4 outlines the studies we will perform in *Xenopus* with the new OCM, searching for the recently reported "vegetal rotation" in early gastrulation that may provide the driving mechanism for the involution of the mesendoderm. We also propose to use our new OCM to resolve unambiguously the question of activity cycles in the *Arabidopsis* shoot apical meristem that arose in our recent OCM studies of phyllotaxis. We will investigate the new *pin* mutant that responds to local application of auxin to the inflorescence meristem by generating an organ.

5. Educational Impact of the Proposed Research

Finally in Section 5 we describe the positive impact of our multidisciplinary OCM project on the quality of the Harvey Mudd educational programs, and on the recruitment and retention of students for careers in science and technology.